Tests of Geoid Height Skill Through Estimates of the Ocean Circulation

Detlef Stammer[1], **Armin Köhl**[1] **and Carl Wunsch**[2]

[1] Institut für Meereskunde, Zentrum für Meeres- und Klimaforschung, Universität Hamburg, Bunderstrasse 53, 20146 Hamburg, Germany; stammer@ifm.zmaw.de; koehl@ifm.zmaw.de

[2] Department of Earth, Atmospheric and Planetary Sciences, Massachusetts Institute of Technology, 77 Massachusetts Avenue, Cambridge MA 02139, U.S.A.; cwunsch@pond.mit.edu

To be submitted to

Journal of Atmosphere and Ocean Technology

Abstract

New geoid height estimates, available from the Gravity Recovery and Climate Experiment (GRACE) spacecraft, are critically assessed with respect to their impact on oceanic state estimation, and the implications of a hypothetical, far more accurate geoid are explored. Circulation estimates were obtained over the period 1992-2002 by combining most of the available ocean data sets with a global general circulation model on a 1^o horizontal grid. The GRACE-based (GGM01s) estimate of the ocean circulation is then compared to that from a previous estimate using the EGM96 geoid model. When combined with altimetric data, the use of the GRACE geoid leads to fields that are more consistent with a temperature and salinity climatology, and the optimization thereby requires smaller adjustments to the initial model conditions, as compared to the EGM96-based solution. The result supports, but does not prove, the inference of greater geoid skill. Oceanographic implications of the changes are comparatively modest—consistent with earlier studies focussed on the time-mean flow alone. To both understand the extent to which the modest shifts are a consequence of a non-fully converged optimization and to understand the impact of a very much more accurate geoid, an additional experiment was performed in which the geoid error was artificially greatly reduced. Adjustments occur then in all aspects of the ocean circulation, including changes in the meridional overturning circulation and the corresponding meridional heat transport in the Atlantic, of about 10% of their mean values. The result shows that the oceanographic implications are quantitatively important, but will be very difficult to be tested by independent means. [Carl: I am not quite convinced by this statement. Maybe it holds in the ocean, but we have argued before that we need OAM or other integral measures (maybe orbit computations) to test our results. We should reiterate this here in the paper.] The error budget of existing time dynamic topography estimates may now be dominated by residual errors in altimetric corrections and these need to be better understood

before even present geoid estimates can be fully used in ocean studies.

1 Introduction

Global state estimation (data assimilation) is becoming a near-routine method for producing dynamically and statistically self-consistent syntheses of models and oceanic data (*Stammer et al.*, 2002a, 2003, 2004; *Köhl et al.*, 2005; Wunsch and Heimbach, 2005). As practiced by these authors, the methodology is a form of constrained least-squares based upon Lagrange multipliers. One of the essential ingredients in carrying out such calculations, as in any least-squares method aiming at a minimum variance estimate, is a quantitative description of the error structure of the data being used. Solutions that are forced closer to observations than is warranted are modeling noise; solutions not close enough to the observations are discarding useful information. Each of the data types used in such calculations has to be examined in detail. A by-product usually is a better understanding of the measurement system itself, and the result can be employed to better interpret the data, even independent of a general circulation model.

Here, we examine the altimetric and geoid components of the state estimates as used in the work of the ECCO (Estimating the Circulation and Climate of the Ocean, *Stammer et al.*, 2002b) Consortium, and its German partner (GECCO). Our specific goals here are three-fold: to understand the changes in the estimates of the ocean circulation imposed by more accurate GRACE geoid fields—measured relative to the previous best-estimate EGM96 geoid (*Lemoine et al.*, 1997); more immediately, to determine the appropriate weights (error variances) that should be used in the state estimates; and to understand the potential impact of improvements in geoid estimates beyond what is possible today. The approach taken is to compare the optimization results from using the different geoids along with all of the other data going into the ECCO/GECCO estimates. The paper is an extension of a previous one (*Köhl et al.*, 2005, referred to as KEA05 hereafter), in which a first ECCO synthesis on a global 1° geographical grid for the period 1992 through 2002 was described which made use of the first geoid esti-

mate derived from the Gravity Recovery and Climate Experiment (GRACE; see Tapley et al., 200x). Wunsch and Heimbach (2005) carried that estimate forward through 2004. *Wunsch and Stammer* (2003) discussed the potential of ocean state estimates as consistency tests.

This note can also be understood as an attempt to extend the existing analyses of the impact of improved geoid estimates on the problem of determining the ocean circulation (Ganachaud et al., 1997; Legrand, et al., 1998; Rio and Hernandez, 2004, among others). These earlier papers focussed, from practical necessity, on the nominally steady-state ocean circulation. Here we extend the discussion to a fully time-dependent system. As will be seen, we have progressed to the point where lack of understanding of data errors seriously inhibits the possibility of making improved estimates of elements of the ocean circulation.

2 Uncertainties in Dynamic dynamic topography Fields

ECCO state estimate efforts are constrained by, among many other data types, the time-mean altimetric dynamic topography, and which is obtained as the difference between mean altimetric observations of the sea surface height (above a reference ellipsoid) minus a geoid height model and its *a priori* error estimate. Accordingly, the error covariance for the surface dynamic topography has to take into account errors in both the geoid and in the altimetric observations. Geoid height errors (which include commission and ommission errors alike) have been previously discussed by various authors. In the past, geoid errors were considered to be the dominant ones. However, with decreasing geoid height errors, the remaining uncertainties in the time-mean and time-varying altimetric data begin to loom large.

Altimetric errors are often conveniently separated into those of the time-mean, and of the temporal anomalies. Unfortunately, the separation is not an absolute one, as the mean continues to be estimated over ever-increasing time intervals and there is no known frequency below which the time-variations in the errors vanish. Chelton et al. (2001) summarize estimates of the

time-mean and total errors as of that time. An updated discussion of the time-variable errors is provided by Ponte and Wunsch (2005) [Is this now the final list of authors?]. We review these results only briefly because of our focus on the geoid error component.

Available altimeter data are currently provided by more than six different altimetric missions including TOPEX/POSEIDON, ERS-1 and -2, ENVISAT, GFO and For many applications, Jason-1. TOPEX/POSEIDON and Jason-1 are the primary data sets, with the instruments having somewhat different designs. Engineering design studies had suggested that the point-errors in both instruments should be 2-3 cm RMS. Note that two instruments with independent white noise errors of 3cm each, should display an RMS white noise difference of $\sqrt{2\,(3)^2} = 4.2$cm. TOPEX/POSEIDON and Jason were kept in essentially identical orbits and locations for 200 days in 2001. The time-mean TOPEX/POSEIDON-Jason differences over this interval are shown in Fig. **??**a (from the NASA Physical Oceanography—Data Archive Center (PODAAC) Fig. **??** data released on 1 February 2004). A considerable spatial structure is visible in the time-mean differences, reiterating however, that 200 days cannot be regarded as accurately representative of the long-term time average. The difference of the anomalies, $\Delta\eta = \eta_T - \eta_J$ for a single 10-day period is shown in Fig. **??**b. The figure displays a similar highly structured field as visible in Fig. **??**a, suggesting that not only the time-mean dynamic topography is corrupted by geographically correlated error signal, but also in each 10-day repeat cycle. More extended discussions of the time-mean errors, insofar as they have been determined, can be found in Beckley et al. (2004), Dorandeu et al. (2004) and Chambers et al. (2004). In addition, a number of regional studies exist.

Table 11 of Chelton et al. (2001) summarizes their global estimates of the RMS altimetric errors as about 4cm, but all published results suggest strong regional variations in this value, perhaps reaching over 10cm in the Southern Ocean. A definitive discussion is impossible at

the present time, and this background altimetric error must be borne in mind in the following discussion of the geoid component.

[To be mentioned: Bosch, (2005)]

3 Methodology

A general circulation model (GCM) is fit by constrained least-squares to a very large data set. Lagrange multipliers are used and the fit is an iterative one (see *Wunsch*, 1996, for details). The underlying model, data, and methodology are described by *Stammer et al.* (2002, 2003) and by *KEA05* who provide further details on the specific model set up and data sets used here. *Lu et al.* (2002) described the input data sets and their prior uncertainties. In brief, the ECCO-GCM is based on the MIT GCM described by *Adcroft et al.* (2002), coupled to a surface mixed layer model (*Large et al.*, 1994), and using the eddy-parameterization scheme of *Gent and McWilliams* (1990). In the present use, horizontal model resolution is 1° over $\pm\ 80^\circ$ in latitude with 23 levels in the vertical, and the estimation period is the 11-years1992-2002.

A schematic of the data constraints is displayed in Fig. 1. Constraints include several satellite data sets (altimetry from TOPEX/POSEIDON, ERS-1 and -2, scatterometer data and Reynolds and microwave SST fields), time-mean surface drifter velocities, in-situ hydrographic temperature and salinity profiles, as well as hydrographic sections. In a first calculation (called *optimization-1*) the difference TP-EGM96 was used to impose constraints on the time-average absolute circulation (see *Köhl et al.*, 2002). A diagonal covariance matrix was used with values taken from the diagonal of the EGM96 error covariance matrix. An estimate of the resulting 11-year time-mean dynamic topography field is displayed in Fig. 2a; Fig. 2b shows the associated residuals relative to the imposed mean dynamic topography of the combined missions (data are all TOPEX/POSEIDON) in the model referred to EGM96. Values are of the order of $\pm$ 20 cm and reach $\pm$50 cm near steep topography. Obvious inconsistencies with the prescribed geoid

Fig. 1

Fig. 2

errors are apparent (compare *Lu et al.*, 2002) and our goal here is to understand those residuals in terms of model and data errors alike.

4 Optimization-2

Because the first optimization revealed large residuals relative to the prior dynamic topography estimate, a second calculation (*optimization-2*) was performed in which all constraints remain the same except that the time-mean TOPEX/POSEIDON dynamic topography field minus the U. of Texas GRACE geoid model (GGM01s; see *Tapley et al.*, 2004) is imposed over the entire 11-year period. We are now basically investigate the question: Does the near-optimized model fit better to the time-mean altimetry based on GRACE than it does to EGM96 assuming the GRACE-Project error estimates are approximately correct?

As an error for the imposed dynamic topography, a geographically uniform value of 4.5cm employed along the covariance matrix diagonal—a smaller value than for EGM96—as advised by the GRACE project. This error can be understood as being composed of roughly 2cm RMS GRACE error plus 2.5 cm RMS mean T/P time-mean error (the latter is very optimistic, especially over the Southern Ocean as discussed above, but only the sum of the errors effects the results). *Optimization-2* was run in parallel to the last six iterations of *optimization-1*, and was extended through 2002 as well. Neither solution is fully converged, but large scale features appear to be relatively insensitive to the continuing slow improvements.

Figs. 3a, b show the contributions to the objective (or misfit or cost) function that remain from the various data sets. Each column was normalized by the corresponding number of data points used and divided by the estimated error variance; the square-root is taken for plotting. Ideally, the results are values whose squares have a mean of one and are distributed in a χ_1^2 distribution. Fig. 3

Figures 3c shows the changes in the RMS model-data misfits of *optimization-2* minus the

results from *optimization-1*, i.e., negative numbers in the figure indicate the improvements of the optimization imposed through the use of the GRACE geoid height. Apparently:

1. Replacing the EGM-96 geoid model by the GRACE one, and reducing the squared error of the dynamic topography to $(4.5cm)^2$ while leaving all other optimization parameters unchanged, produces a new solution significantly closer to the initial conditions of the *Levitus et al.* (1994) climatological temperature (T) and salinity (S) fields. Although, this improvement could be a coincidence, it can be interpreted as supporting the inference that the GRACE geoid is oceanographically more accurate.

2. A reduction in the vertical velocity drift during *optimization-2* indicates that the initial conditions from *optimization-2* are closer to being dynamically balanced than was the case in *optimization-1*. At the same time, misfits between the monthly-mean climatological hydrographic fields from *optimization-2* and climatological fields are smaller, as are most of the misfits to temperature profile data sets, such as XBTs, ARGO and CTD data. As with (1), the result is consistent with the new geoid being an improvement.

The time-mean misfit of the dynamic topography, however, increases with the use of the GRACE geoid. This increase is apparently primarily due to the reduced error imputed to the new geoid (that is, because the misfit terms are divided by a smaller number). Nonetheless, the absolute (unweighted) misfit decreases as shown in Fig. 4a. These residuals are much smaller than those found from *optimization-1* (compare Fig. 2b), implying that the GRACE geoid is closer to dynamical consistency with the GCM and other data than is EGM96. The dynamic topography misfit in *optimization-2* shows residuals of the order of $\pm$10cm and reaches $\pm$40cm on relatively short spatial scales near steep topography, especially over the Southern Ocean. The implication is that the 4.5cm RMS error remains unrealistically optimistic in those regions and that a full error covariance budget for the dynamic sea surface height is required—one that

Fig. 4

would have strong spatial variability. Current optimization weights are based upon calculations similar to that in Fig. 4 with strongly varying misfits permitted.

Fig. 4b, showing the differences in the estimated time-mean dynamic topography obtained from *optimization-2* minus that of *optimization-1*, illustrates that adjustments in dynamic topography forced in *optimization-2* relative to those in *optimization-1* are small. Large-scale changes are typically only of the order of 1cm or less, and arise from optimization changes in temperature and salinity (not shown) of the order of $\pm 1^\circ$ and 0.1 respectively, depending on the depth, bringing the second optimization closer to the hydrographic climatology. Maximum differences of $\pm$5cm are reached only in two regions—in the Antarctic Circumpolar Current south of New Zealand and in the North Atlantic.

5 Optimization-3: Impact of a Hypothetical Accurate Geoid

The question arises as to whether the comparatively modest changes in the circulation owing to the use of the new geoid arise because the information content in the geoid relative to other data is comparatively low (e.g., Ganachaud et al., 1997; Legrand et al., 1998), or whether it is simply the failure to bring the system to the asymptotic, fully optimized, state. One would especially like to know whether a hypothetically far more accurate geoid would also make a major difference in estimating the ocean circulation. In an attempt to distinguish these possibilities, *optimization-2* was continued as *optimization-3*, with the geoid height error kept fixed, but with the weights of all remaining misfit terms reduced significantly to force the solution closer to the GRACE geoid estimate (in least-squares only the relative errors matter).

To this end we artificially force the model to the time-mean dynamic topography by increasing the relative errors on the non-geoid misfit terms by a factor of 12 during 10 further iterations, and then by a factor of 50 during a final 9 iterations. This optimization essentially addresses the question raised by Ganachaud et al. (1997) of the extent to which a *much* improved geoid

estimate would carry information about the ocean circulation not already contained in other data and in the model physics themselves. Resulting contributions to the objective function are displayed in Figures 3b (to compare this with the contributions of *optimization-2* we use the error weights of optimzation-2 in both). Figure 3d shows changes in the RMS misfits of *optimization-3* minus the results from *optimization-1*.

Complex shifts take place in the absolute misfits of the remaining data. For example, there is improvement and degradation of temperature and salinity misfits averaging nearly to zero, except that the misfits to all vertical profile data decreased. Seasurface salinity misfits are improved, but the deep salinity misfits degrade. These changed misfits are difficult to interpet, as they depend upon the detailed nature of the real errors in the GRACE geoid as well as inaccuracies in the remaining data types. Their significance is two-fold: their orders of magnitude and spatial structure show what can be interpreted as a scale analysis of the impact of a better geoid, and they show how difficult it will be to confirm by independent means their oceanographic implications. We discuss separately changes implied by the imposed geoid in the control terms and in the ocean state itself.

5.1 Changes in Control Terms

Changes in the estimated circulation and integral transport quantities shown below between *optimization-3* minus *optimization-1* are enforced by changes in the control terms of the optimizations. Corrections to initial conditions for temperature and salinity are significantly increased in *optimization-3*. The increase is mainly noticeable in the abbysal Antarctic Circumpolar Current (ACC) region. Fig. 5 shows a section along 60 $^\circ$ N of the changes in temperature (top) and salinity (bottom). Most noticeable are changes directly adjacent to strong topographical slopes which indicate that interaction with bottom topography is the main agent bringing the model into consistency with the new mean dynamic topography field. The remaining control

Fig. 5

parameters are the time-varying surface forcing fields of net heat and freshwater fluxes and wind stress. Fig. 6 shows the time-mean changes in surface forcing fields between *optimization-3* and *optimization-1*. Peak changes in estimated heat flux, freshwater flux and wind stress are 14 W/m^2, 0.03 m/yr and 0.005 Nm^2, respectively. All changes are oceanographically improtant, and it is important to be aware that carrying the optimization further would likely lead to even larger changes. Fig. 6

For net heat and freshwater fluxes, roughly the same patterns emerge. Altough changes in heating and freshwater fluxes tend to oppose each other in the density field, heat flux changes dominate by an order of magnitude. The largest adjustments occur along major current systems, including the Kuroshio, Gulf Stream and ACC. We note that the estimated changes of the zonal wind stress relative to the NCEP first guess are in part enhancements in the changes made previously in optimization-1, with some new elements (especially in the Indian and Pacific Ocean). The main conclusion drawn here is that a high accuracy geoid would provide information about oceanic surface boundary conditions, although we recall that due to the specifics of the set-up of this experiment, the particular shifts found here have no significance beyond their existence and magnitude. In essence, they illustrate the impact on the ocean circulation estimate that could be expected from better geoid and dynamic topography fields.

5.2 Circulation Changes

Changes in the estimated circulation are forced by the differences in the estimated mean dynamic topography. As with the control terms, the main information lies with the estimates of the magnitudes of the inferred changes, rather than with the spatial specifics—which again, depend on elements of the geoid believed to be largely erroneous. Fig. 7 shows the dynamic topography residual before and after *optimization-3* relative to the TOPEX/POSEIDON-GGM02C geoid model. Differences diminish from the order of 10 cm to, typically, a few cm. Fig. 7

Although larger-scale gyre structures are adjusted, residuals remain on small spatial scales and along boundaries, as expected given the absence of those scales in the geoid height. Differences also persist throughout the ACC, whereas the largescale background of the dynamic topography model-data difference is removed and only the chain of positive anomalies of positive anomalies, though reduced, remain. Fig. 7 shows that increasing the relative weight of the time-mean dynamic topography leads to a significantly changed time-mean dynamic topography estimate. The related change in the flow field is demonstrated in Fig. 8 which shows the difference in the time mean dynamic topography estimates between *optimization-3* minus *optimization-1*. In contrast to *optimization-2*, changes are now of the order of $\pm$ 10cm. Maximum amplitudes occur in the western tropical Pacific, the North Pacific, the subtropical and subpolar North Atlantic and along the ACC. In its lower panel, the figure shows changes in the barotropic steam function. Regionally, changes are of the order of $\pm$ 5 Sv, e.g., in the North Atlantic. Drake Passage transports diminished by 4 Sv. Further details are provided in Table 1. Fig. 8

Changes in time-mean temperature and salinity from 200 m depth are shown in Fig. 9 . The lower panels of the figure show vertical sections through the Atlantic along 30°W. T and S changes are greatest near the surface, but that they also have large vertical extent in the subpolar gyre. Differences in the flow field are illustrated in Fig. 10 for changes in the zonal velocity component along sections along 180° E and 30° W. Shifts in the zonal velocity field show a clear vertical coherence and are quite pronounced in the ACC and in the subpolar North Atlantic (of order 3cm/s). The same figure shows changes in the horizontal velocity field between 200 and 2000m depth of the North Atlantic. Maximum changes are of the order of 3cm/s and 1cm/s in amplitude. The velocity pattern indicates a northward shift of the Gulf Stream and a weaker slope water flow in *optimization-3* near the surface. Fig. 9 Fig. 10

All these changes have measurable consequences for transports, e.g., changes imposed by the new geoid are potentially measurable in a reduced deep western boundary current (Fig. 10),

a weaker MOC in the upper North Atlantic Deep Water branch for *optimization-3* relative to *optimization-1* (by about 2 Sv; or about 10% of the mean value) (Fig. 11a). However, the deep cell (below 2000m) is enhanced in the North Atlantic and decreased in the South Atlantic. Establishing field programs to demonstrate their reality would not, however, be cheap or easy. Fig. 11

In the lower panel, Fig. 11 shows the changes in the time-mean global meridional heat transport. Again changes are of the order of 10% of the local time mean value. Like MOC changes, maximum heat transport changes occur in the southern hemisphere, where increased southward (poleward) heat transport by up to 0.05 PW can be observed. Contributions from each of the oceans are of the same order but compensate each other partly.

The implications of this experiment are that if the accuracy of the GRACE-based dynamic surface topography were significantly better than now estimated, that quantitatively improved ocean circulation estimates would be obtained. If one simply assumed that the present GRACE geoid estimate were much more accurate than its authors believe, one could not test the oceanographic implications: there is no independent measure of the circulation differences implied. However, remaining residuals near the boundaries and in the ACC indicate, particularly, the continued importance of the omission errors of the GRACE geoid—the missing short scales.

6 Discussion

Comparisons of the oceanographic implications of the EGM96 versus GRACE geoids for estimates of the ocean circulation, support the inference that the GRACE geoid has a significantly improved skill (as compared to EGM96) on spatial scales of 500 km and larger. The apparent improvement has measurable, if weak, oceanographic and climate consequences consistent with the earlier inferences based upon steady-state assumptions. In particular, the GRACE geoid appears to be more consistent with temperature and salinity climatologies than is the older geoid, although this improvement is not definitive, given issues concerning the climatology accuracies.

The new geoid requires smaller adjustments to the initial model conditions (from Levitus et al., 1994). At present levels of accuracy, the GRACE geoid height estimates, while apparently an improvement over EGM96, do not lead to qualitative shifts in the estimated ocean circulation.

The implications of a much improved geoid (beyond that now available from GRACE) can be explored by driving the model arbitrarily close to the existing geoid, as though it were extremely accurate. Forcing such a fit produces structures in the inferred general circulation which are significantly different from those estimated using a realistic error estimate. There is no oceanographic reason to reject these structures—they are oceanographically reasonable—because there is no independent test of their reality. We seemingly have reached a stage with combined altimetry/geodesy in which further geoid improvement could significantly improve estimates of the ocean circulation. Whether such further improvement relative to the errors of the other data types is possible is unclear at the present time.

A critical issue remains the need to better discriminate between errors in the altimetric and geoid estimates neither of which is well understood at the levels of accuracy now apparently being achieved by ECCO-like estimation procedures. The results here suggest that a spatially uniform error in the existing GRACE geoid, as suggested by the project, is qualitatively incorrect in many locations. As discussed above, the many elements of the altimetric error also appear to have strong spatial variability and the separation of time-mean and time-varying errors remains incomplete.

Acknowledgments. Discussions with R. Ponte were helpful. The authors thank D. Chambers who provided the mean dynamic TOPEX - GRACE topography field relative to the geoid models GGM01s and GGM02c. C. King helped with the processing of TOPEX/POSEIDON and JASON data. Re-analysis surface forcing fields from the National Center for Environmen-

tal Prediction/National Center for Atmospheric Research (NCEP/NCAR) are obtained through a computational grant at NCAR. Computational support from the National Partnership for Computational Infrastructure (NPACI) and the National Center for Atmospheric Research (NCAR) is acknowledged. The TAF software tool was used to create the adjoint of the ECCO forward model code. Supported in part through ONR (NOPP) ECCO grants N00014-99-1-1049 and N00014-99-1-1050, through NASA grants NAG5-XXXX and NAG5-YYYY. This is a contribution of the Consortium for Estimating the Circulation and Climate of the Ocean (ECCO) funded by the National Oceanographic Partnership Program.

References

[1] Adcroft A. and Campin J.-M. and Heimbach P. and Hill C. and Marshall J., 2002: Mitgcm Release 1. http://mitgcm.org/sealion/.

[2] Beckley, B. D., N. P. Zelensky, S. B. Luthcke, and P. S. Callahan, 2004: Towards a seamless transition from TOPEX/Poseidon to Jason-1. *Mar. Geod.*, 27, 373-389.

[3] Chelton, D.B., J.C. Ries, B.J. Haines, L.-L. Fu, and P.S. Callahan, Satellite Altimetry. In *Satellite Altimetry and Earth Sciences*, L.-L. Fu and A. Cazenave (ed.), p. 1 – 131, 2001.

[4] Ganachaud, A., C. Wunsch, M.-C. Kim, and B. Tapley, 1997 Combination of TOPEX/POSEIDON data with a hydrographic inversion for determination of the oceanic general circulation. *Geophys. J. Int'l.*, 128, 708-722

[5] Gent, P. R., and J. C. McWilliams, 1990: Isopycnal mixing in ocean models. *J. Phys. Oceanogr.*, 20, 150-155.

[6] Giering, R., and T. Kaminski, 1998: Recipes for adjoint code construction, *Association for Computing Machinery Transactions on Mathematical Software*, **24**, 437–474.

[7] Gilbert, J.C., and C. Lemaréchal, Some numerical experiments with variable-storage quasi-Newton algorithms, *Mathematical Programming* 45, p. 407-435, 1989.

[8] Kalnay, E., M. Kanamitsu, R. Kistler, W. Collins, D. Deaven, . Gandin, M. Iredell, S. Saha, G. White, J. Woollen, Y. Zhu, M. Chelliah, W. Ebisuzaki, W. Higgins, J. Janowiak, K. C. Mo, C. Ropelewski, A. Leetmaa, R. Reynolds, and R. Jenne, 1996: The NCEP/NCAR re-analysis project. *Bull. Amer. Meteor. Soc.*, 77, 437-471.

Koehl, A., Y. Lu, P. Heimbach, B Cornuelle, D. Stammer, C. Wunsch and the ECCO Consortium: The ECCO 1 degree global WOCE Synthesis. ECCO Reprort Series, Report No.20, November 2002.

[9] Köhl, A., D. Stammer and B. Cornuelle, 2004: Interannual to decadal changes in the global ECCO WOCE synthesis. Submitted for publications.

[10] Large, W. G., J.C. McWilliams, and S.C. Doney, 1994: Oceanic vertical mixing: a review and a model with nonlocal boundary layer parameterization, *Rev. Geophys.*, 32, 363–403.

[11] LeGrand, P., H. Mercier, and T. Reynaud 1998 Combining T/P altimetric data with hydrographic data to estimate the mean dynamic topography of the North Atlantic and improve the geoid*Ann. Geophysicae*, 16, 638-650

[12] Losch, M. and J. Schröter, 2004: Estimating the circulation from hydrography and satellite altimetry in the Southern Ocean: limitations imposed by the current geoid models *Deep-Sea Res. I*, 51, 1131-1143.

[13] Lemoine, F. and 17 others The development of the NASA GSFC and NIMA Joint Geopotential Model. in, *Proceedings of the International Symposium on Gravity*, Geoid and Marine Geodesy, IAG Symposium: in press H. Fujimoto, ed. Springer-Verlag, 1997.

[14] Levitus, S., R. Burgett, and T. Boyer, *World Ocean Atlas 1994*, vol. 3, *Salinity*, and vol. 4, *Temperature, NOAA Atlas NESDIS 3 & 4*, U.S. Dep. of Comm., Washington, D.C., 1994.

[15] Levitus, S, J. I. Antonov , T. P. Boyer , C. Stephens:Warming of the world ocean, *Science*, 287 , 2225–2229, 2000.

[16] Lu, Y., K. Ueyoshi, A. Köhl, E. Remy, K. Lorbacher and D. Stammer: Input Data Sets for the ECCO Global 1° WOCE Synthesis. ECCO Report Series; Report No.18, August 2002.

[17] Marotzke, J., R. Giering, Q. K. Zhang, D. Stammer, C. N. Hill, and T. Lee, 1999: Construction of the adjoint MIT ocean general circulation model and application to Atlantic heat transport sensitivity, *J. Geophys. Research*, 104, 29,529 - 29,548, 1999.

[18] Ménard, Y., L.-L. Fu, P. Escudier, F. Parisot, Jperbos, P. Vincent, S. Desai, B. Haines and G. Kunstmann, 2003: The Jason-1 Mission. *Mar. Geod.*, 26, 131-146.

[19] Rio, M. H. and F. Hernandez 2004 A mean dynamic topography computed over the world ocean from altimetry, in situ measurements, and a geoid model *J. Geophys. Res.*, 109, C12032.

[20] Stammer, D., C. Wunsch, R. Giering, C. Eckert, P. Heimbach, J. Marotzke, A. Adcroft, C.N. Hill, and J. Marshall, 2002, The global ocean circulation during 1992 –1997, estimated from ocean observations and a general circulation model, *J. Geophys. Res.*, 107(C9), 3118, doi:10.1029/2001JC000888.

[21] Stammer, D., C. Wunsch, R. Giering, C. Eckert, P. Heimbach, J. Marotzke, A. Adcroft, C.N. Hill, and J. Marshall, 2003: Volume, Heat and Freshwater Transports of the Global Ocean Circulation 1993 –2000, Estimated from a General Circulation Model Constrained by WOCE Data, *J. Geophys. Res.*, VOL. 108(C1), 3007, doi:10.1029/2001JC001115.

[22] Stammer, D., K. Ueyoshi, A. Köhl, W.B. Large, S. Josey and C. Wunsch, 2004: Estimating Air-Sea Fluxes of Heat, Freshwater and Momentum Through Global Ocean Data Assimilation, *J. Geophys. Res.*, 109, C05023, doi:10.1029/2003JC002082.

[23] Tapley, B.D, D. P. Chambers, S. Bettadpur, and J. C. Ries, 2003. Large Scale Ocean Circulation from the GRACE GGM01 Geoid, Geophys. Res. Ltrs, 30(22), 2163, doi:10.1029/2003GL018622.

[24] Wunsch, C. and P. Heimbach, 2005. Practical global oceanic state estimation. Submitted for publication.

Figure Captions

1. The upper part shows the data constraints imposed on the model during *optimization-1*. The lines indicate times where data is available, mean or climatological data is shown as available throughout the whole period. The lower part summarizes the "control variables" that were changed during the optimization.

2. Time-mean seasurface height (dynamic topography) as it results from the 11-year *optimization-2*, relative to the EGM-96 geoid (*Lemoine et al.*, 199?). (lower panel) Optimized dynamic topography differences with respect to T/P-EGM96. Contour interval is 10cm. This field can be regarded as an ECCO-computed adjustment to the geoid to render it consistent with the model and other data.

3. top: Objective function contributions from individual data sets for the optimized state taken from *optimization-2* (left) and *optimization-3* (right). In the upper panel bars represent values for the optimized state after normalization with the number of observations. In a fully optimized, consistent result, the square-root value of all of these bars should have magnitude one. In the lower panel the changes of each bar between the GRACE and the EGM96 optimizations are displayed. Negative values indicate an improvement in the quadratic model-data misfit for each variable

4. Changes to the initial conditions in temperature (top in $^\circ$ C) and salinity (bottom, on the practical salinity scale) along 60 $^\circ$ S.

5. Differences in the forcing corrections between optimization-3 and optimization-1. Shown are the mean heat flux (W/m^2, top left), mean freshwater flux (mm/yr,top right), and the mean zonal (lower left) and meridional (lower right) wind stress in mN/m^2. [We should adjust the colorbar and highlight the zero line. Is positive more or less heat/freshwater

into the ocean?]]

6. Differences in the time-mean dynamic topography in cm between the field from *optimization-2* and the GRACE dynamic topography and between *optimization-2* and *optimization-1* (lower).

7. Differences in the time-mean dynamic topography in cm between the field from *optimization-2* and the GRACE dynamic topography (upper) and between *optimization-3* and the GRACE dynamic topography (lower).

8. (top) Differences in the time-mean dynamic topography in cm between *optimization-3* and *optimization-1*. (bottom) Differences in the barotropic stream function between optimization-3 and optimization-1 (Units are Sv). .

9. Differences in the time-mean temperature (left, in ° C) and salinity (right, practical salinity scale) between optimization-3 and optimization-1 in 200m depth (top row) and at 30^{o}E (bottom row).

10. Differences in the time-mean velocities between the optimization-3 and optimization-1. Zonal velocity differences at plotted in the top left and top right panels along 180^{o}W and 30^{o}E, respectively. CI are XX cm/s. In the lower panels velocity differences are plotted as they result in 200m and 2000m depth (lower left and right panels), respectively. Reference arrows show speeds of 2 cm/s and 0.5 cm/s.

11. Differences in (top) the global meridional overturning stream function (in Sv) and (bottom) the global meridional heat transport (in PW) between optimization-3 and optimization-1.

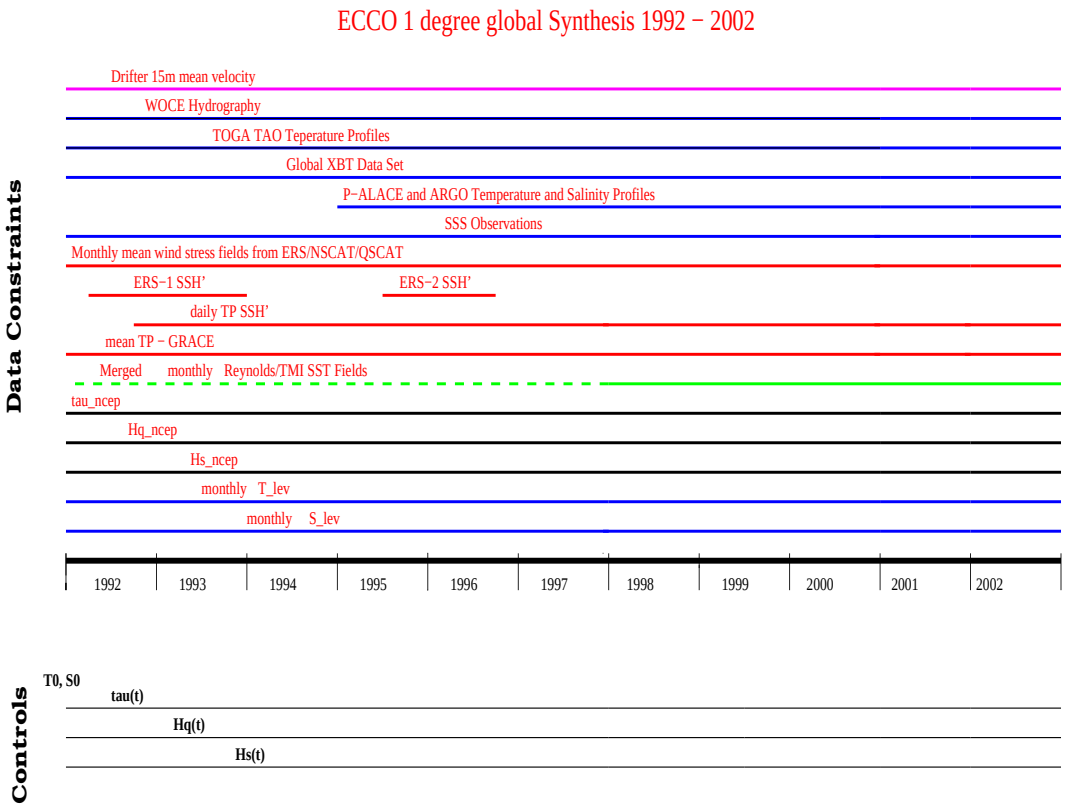
ECCO 1 degree global Synthesis 1992 − 2002
Data Constraints
Drifter 15m mean velocity
WOCE Hydrography
TOGA TAO Teperature Profiles
Global XBT Data Set
P−ALACE and ARGO Temperature and Salinity Profiles
SSS Observations
Monthly mean wind stress fields from ERS/NSCAT/QSCAT
ERS−1 SSH'
ERS−2 SSH'
daily TP SSH'
mean TP − GRACE
Merged monthly Reynolds/TMI SST Fields
tau_ncep
Hq_ncep
Hs_ncep
monthly T_lev
monthly S_lev
1992
1993
1994
1995
1996
1997
1998
1999
2000
2001
2002
Controls
T0, S0
tau(t)
Hq(t)
Hs(t)

Figure 1:

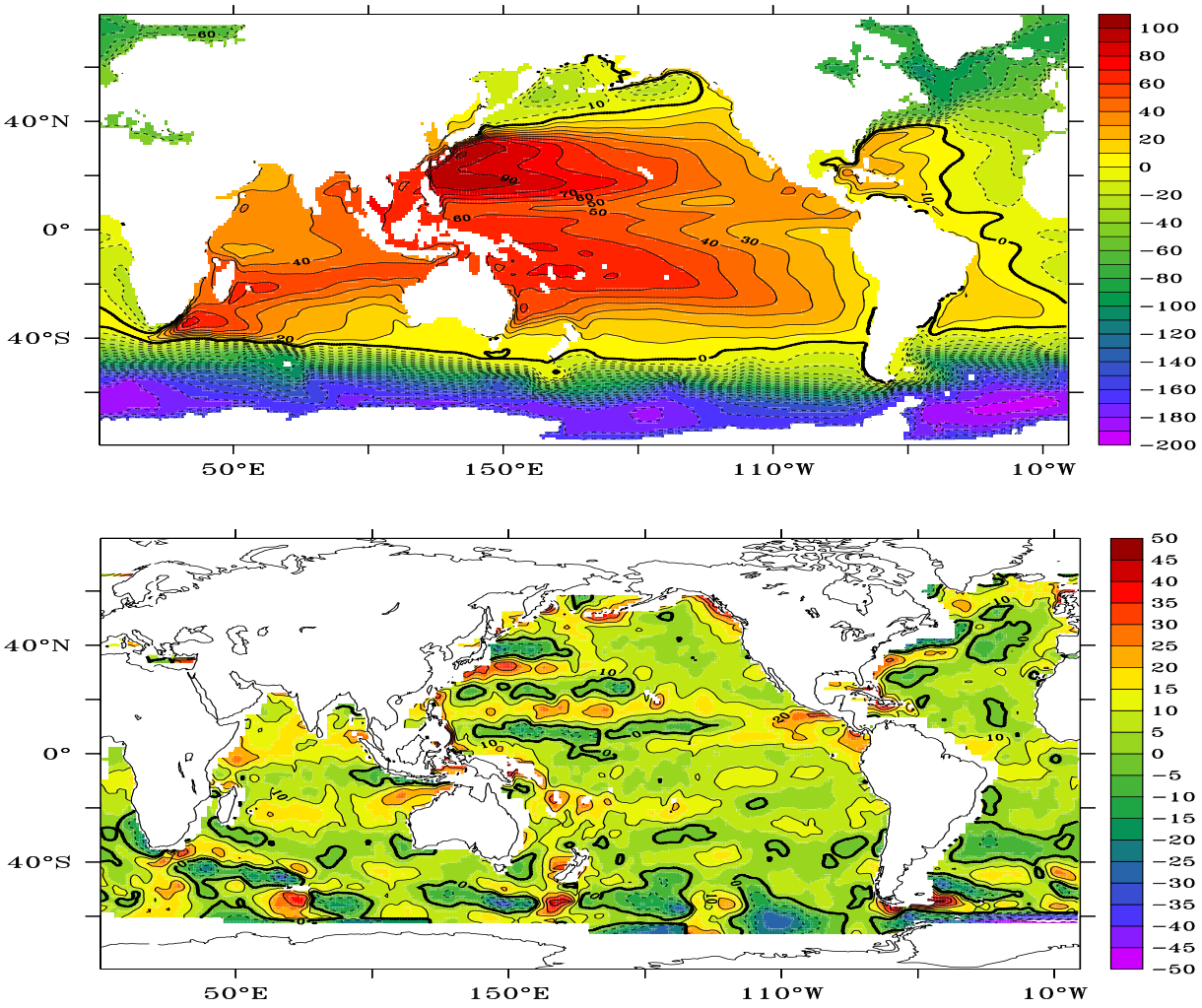
40°N
0°
40°S
50°E
150°E
110°W
10°W
100
80
60
40
20
0
−20
−40
−60
−80
−100
−120
−140
−160
−180
−200
40°N
0°
40°S
50°E
150°E
110°W
10°W
50
45
40
35
30
25
20
15
10
5
0
−5
−10
−15
−20
−25
−30
−35
−40
−45
−50

Figure 2:

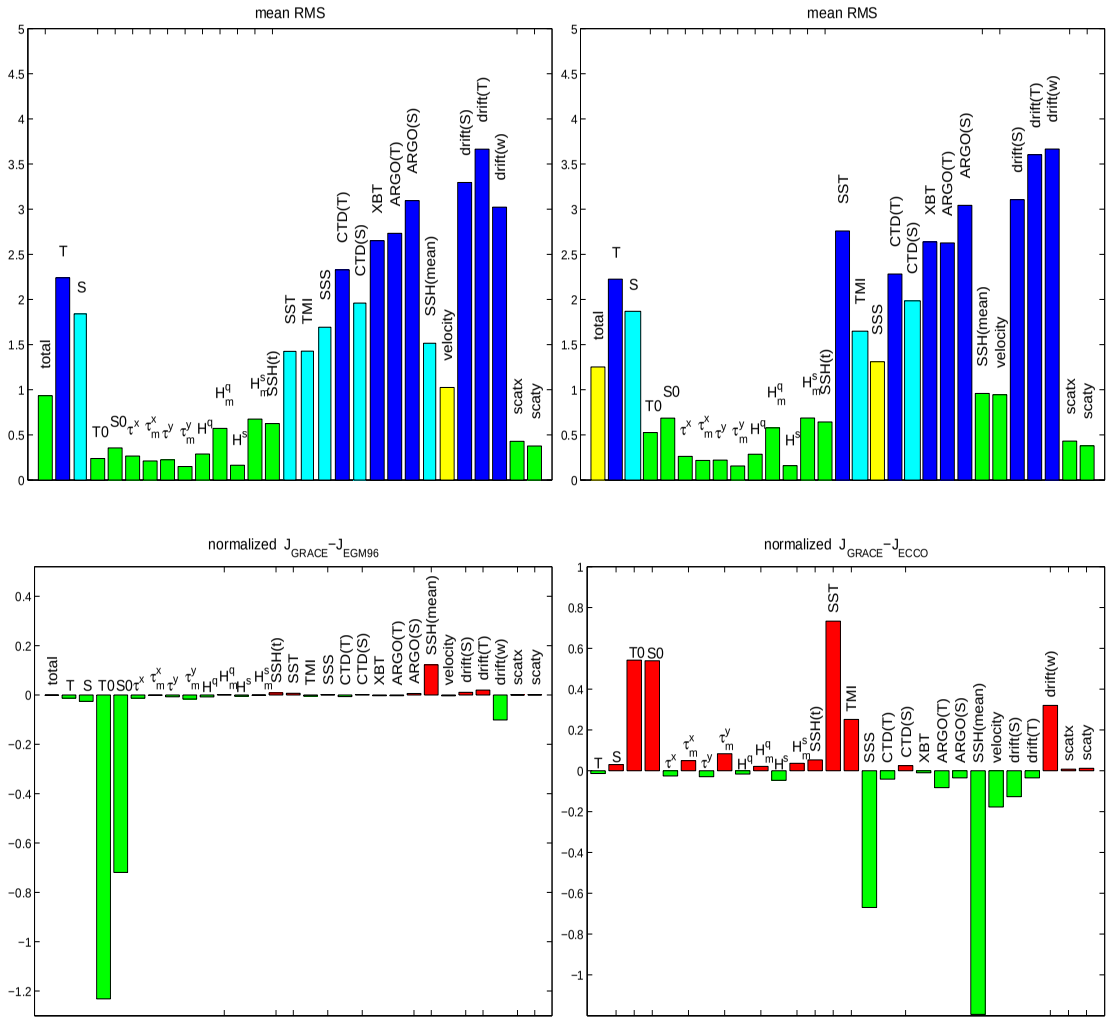
mean RMS
mean RMS
normalized J_GRACE−J_EGM96
normalized J_GRACE−J_ECCO
total
T
S
T0
S0
SST
TMI
SSS
CTD(T)
CTD(S)
XBT
ARGO(T)
ARGO(S)
SSH(mean)
velocity
drift(S)
drift(T)
drift(w)
scatx
scaty

Figure 3:

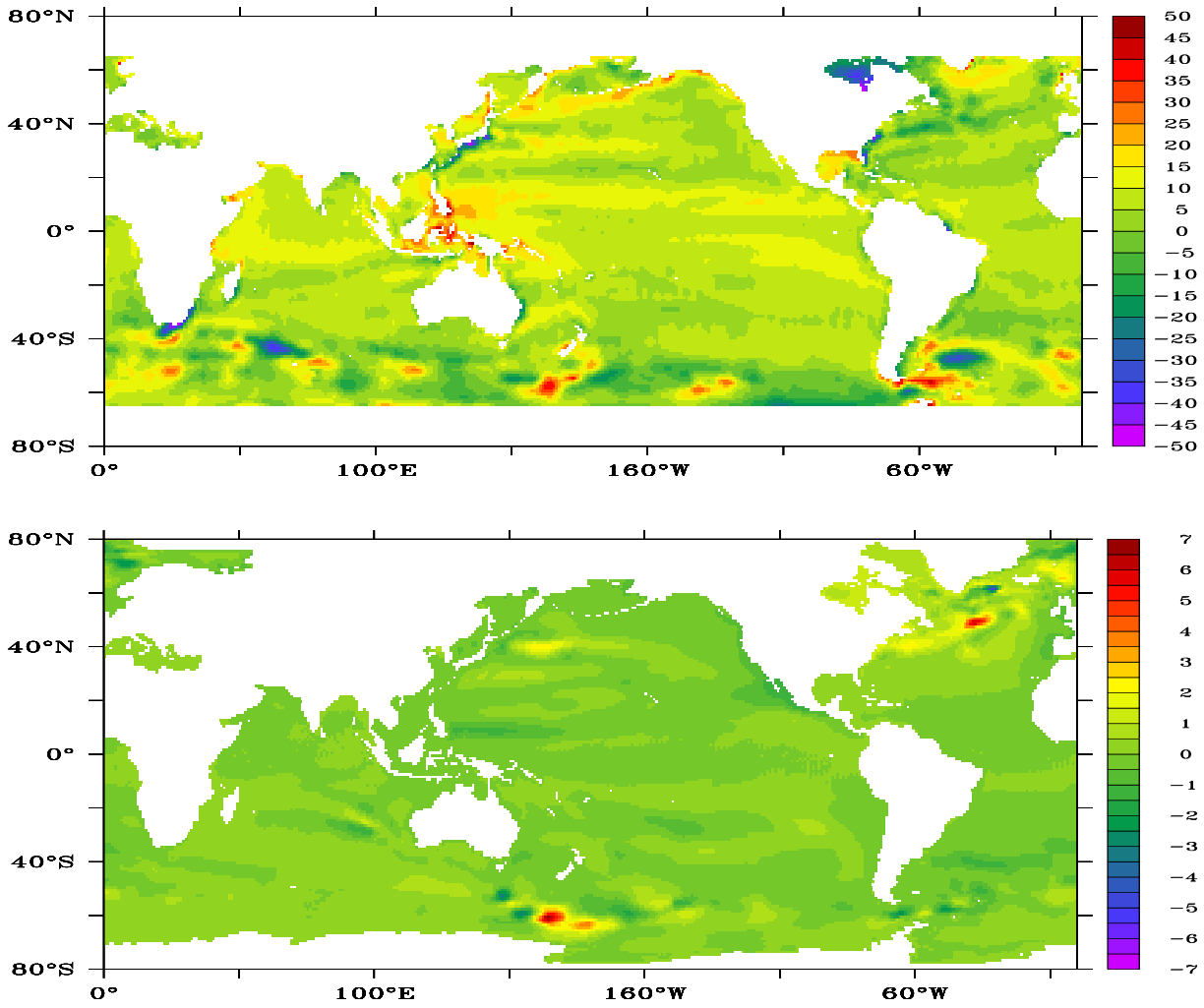
80°N
40°N
0°
40°S
80°S
0°
100°E
160°W
60°W
50
45
40
35
30
25
20
15
10
5
0
−5
−10
−15
−20
−25
−30
−35
−40
−45
−50
80°N
40°N
0°
40°S
80°S
0°
100°E
160°W
60°W
7
6
5
4
3
2
1
0
−1
−2
−3
−4
−5
−6
−7

Figure 4:

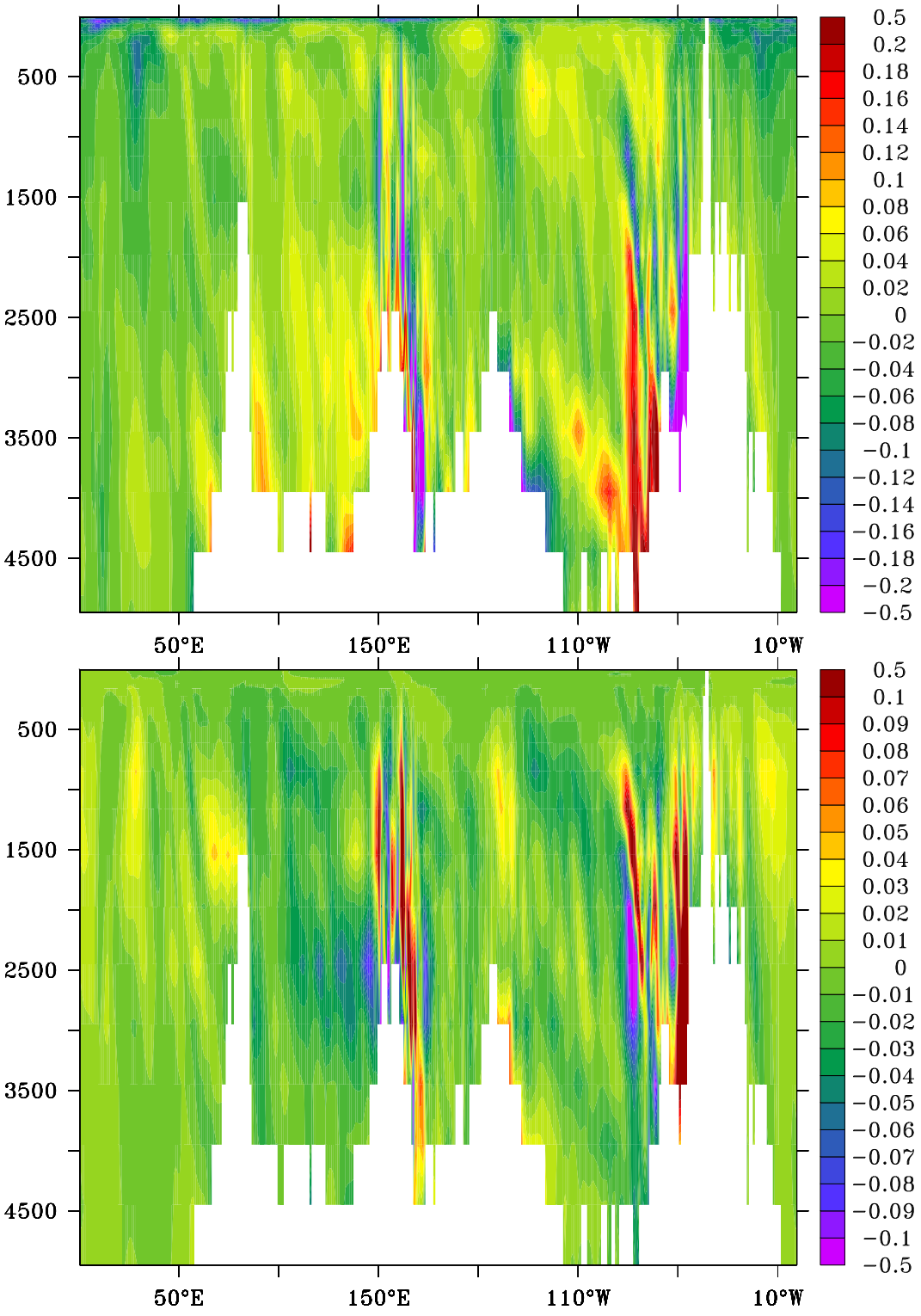
500
1500
2500
3500
4500
50°E
150°E
110°W
10°W
0.5
0.2
0.18
0.16
0.14
0.12
0.1
0.08
0.06
0.04
0.02
0
−0.02
−0.04
−0.06
−0.08
−0.1
−0.12
−0.14
−0.16
−0.18
−0.2
−0.5
500
1500
2500
3500
4500
50°E
150°E
110°W
10°W
0.5
0.1
0.09
0.08
0.07
0.06
0.05
0.04
0.03
0.02
0.01
0
−0.01
−0.02
−0.03
−0.04
−0.05
−0.06
−0.07
−0.08
−0.09
−0.1
−0.5

Figure 5:

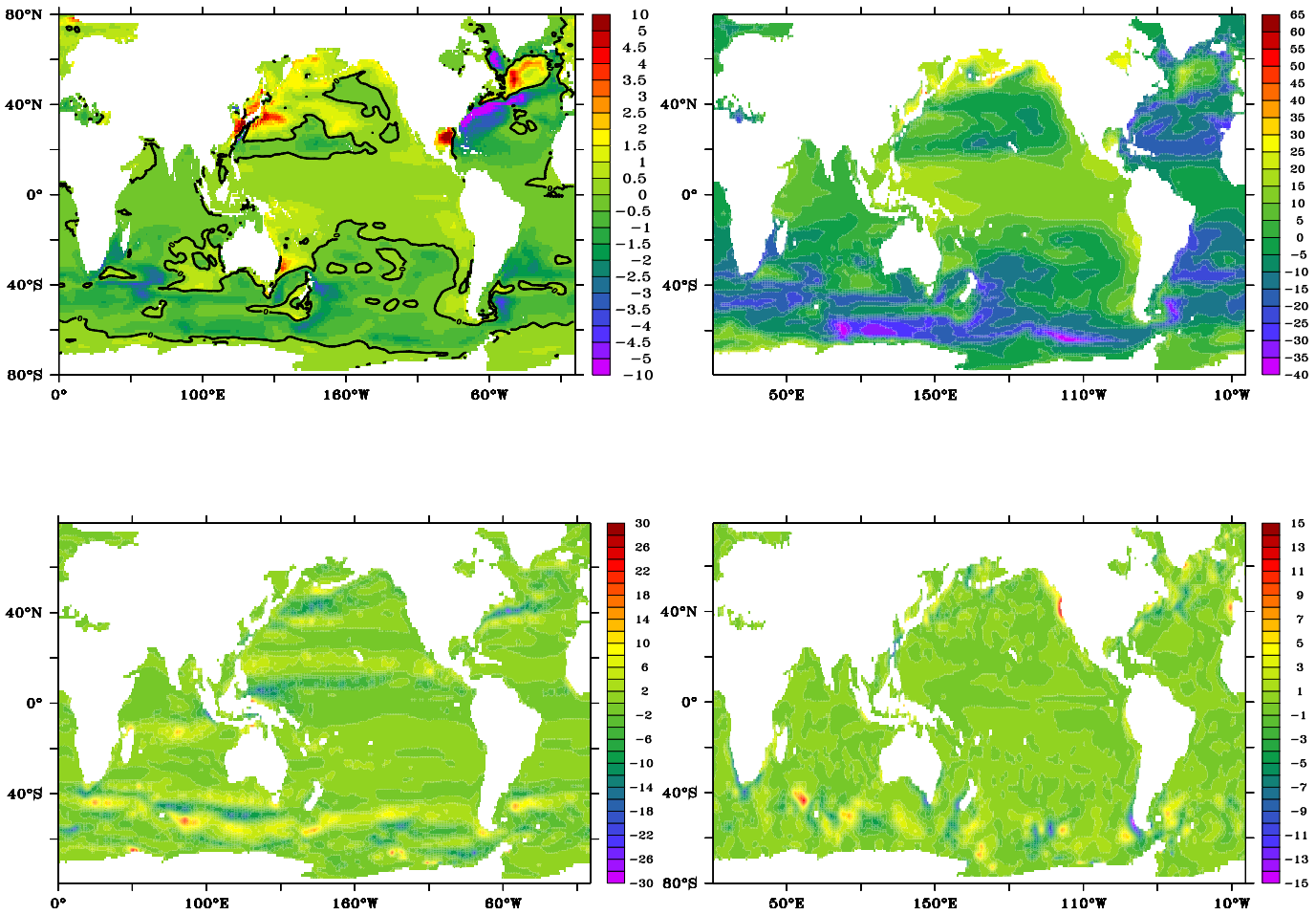
80°N
40°N
0°
40°S
80°S
0°
100°E
160°W
60°W
10 5 4.5 4 3.5 3 2.5 2 1.5 1 0.5 0 −0.5 −1 −1.5 −2 −2.5 −3 −3.5 −4 −4.5 −5 −10
40°N
0°
40°S
50°E
150°E
110°W
10°W
65 60 55 50 45 40 35 30 25 20 15 10 5 0 −5 −10 −15 −20 −25 −30 −35 −40
40°N
0°
40°S
0°
100°E
160°W
60°W
30 26 22 18 14 10 6 2 −2 −6 −10 −14 −18 −22 −26 −30
40°N
0°
40°S
80°S
50°E
150°E
110°W
10°W
15 13 11 9 7 5 3 1 −1 −3 −5 −7 −9 −11 −13 −15

Figure 6:

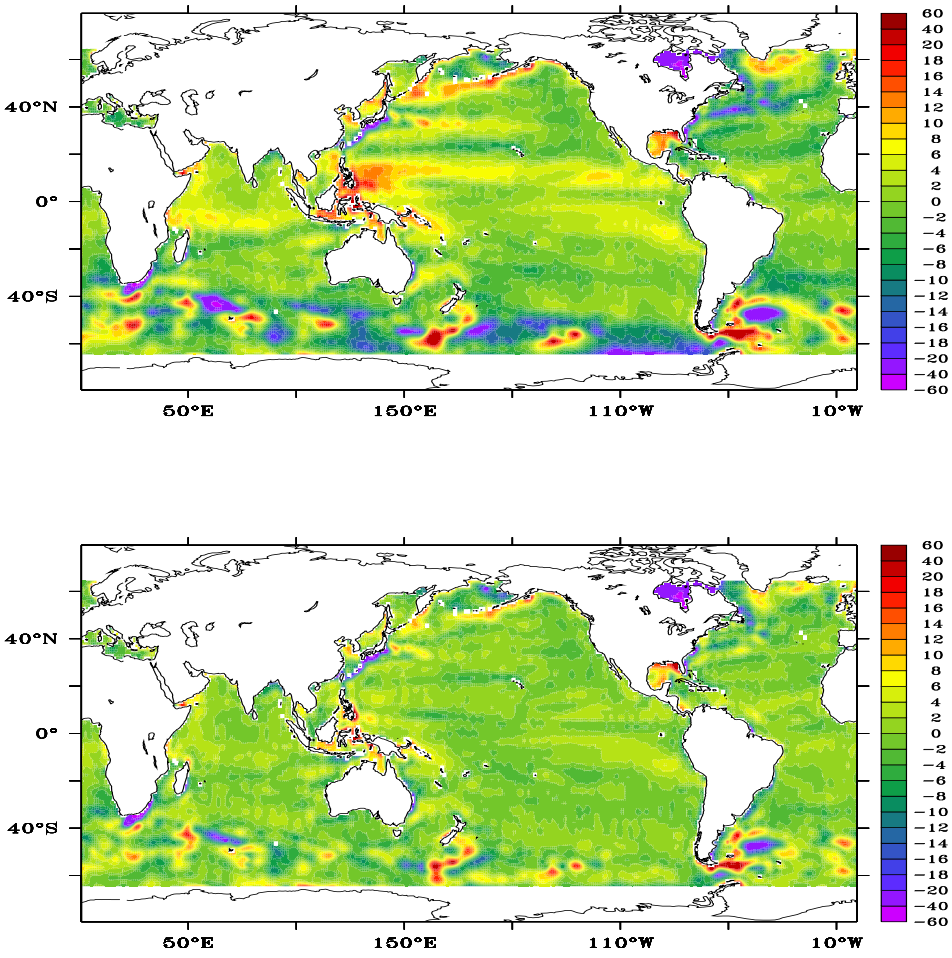
40°N
0°
40°S
50°E
150°E
110°W
10°W
60
40
20
18
16
14
12
10
8
6
4
2
0
−2
−4
−6
−8
−10
−12
−14
−16
−18
−20
−40
−60

Figure 7:

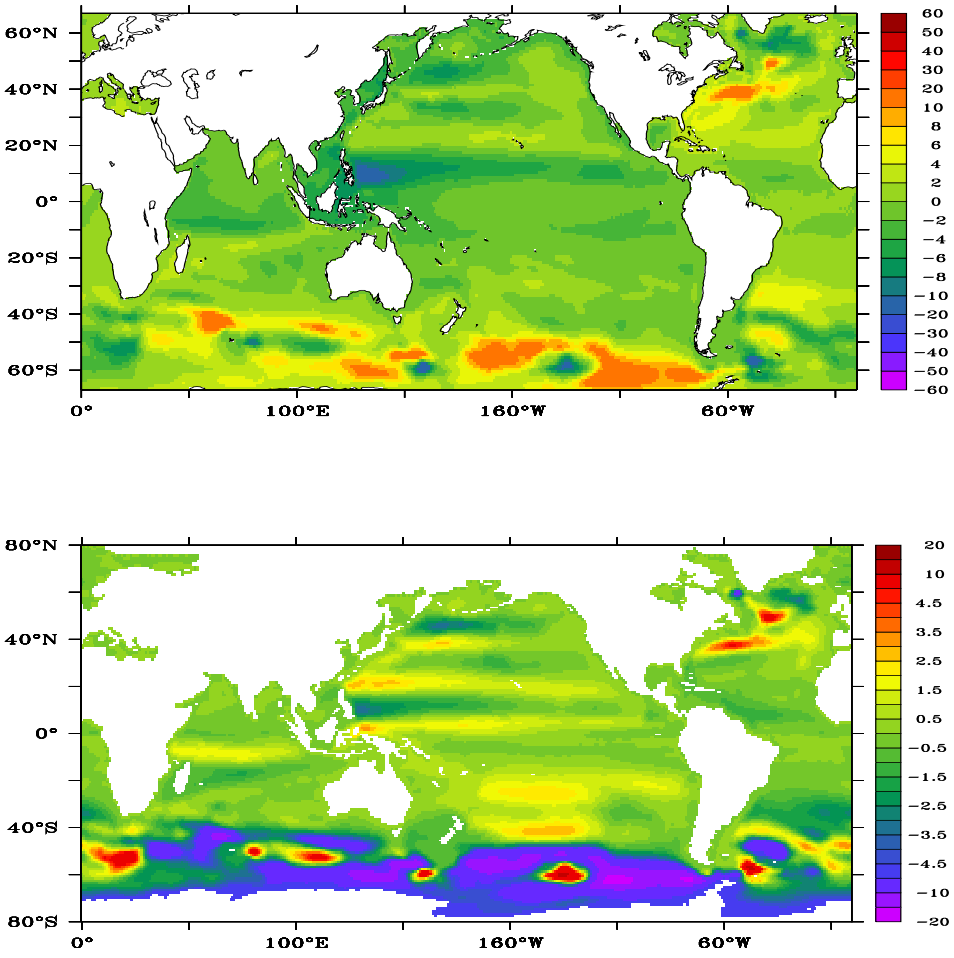
60°N
40°N
20°N
0°
20°S
40°S
60°S
0°
100°E
160°W
60°W
60
50
40
30
20
10
8
6
4
2
0
−2
−4
−6
−8
−10
−20
−30
−40
−50
−60
80°N
40°N
0°
40°S
80°S
0°
100°E
160°W
60°W
20
10
4.5
3.5
2.5
1.5
0.5
−0.5
−1.5
−2.5
−3.5
−4.5
−10
−20

Figure 8:

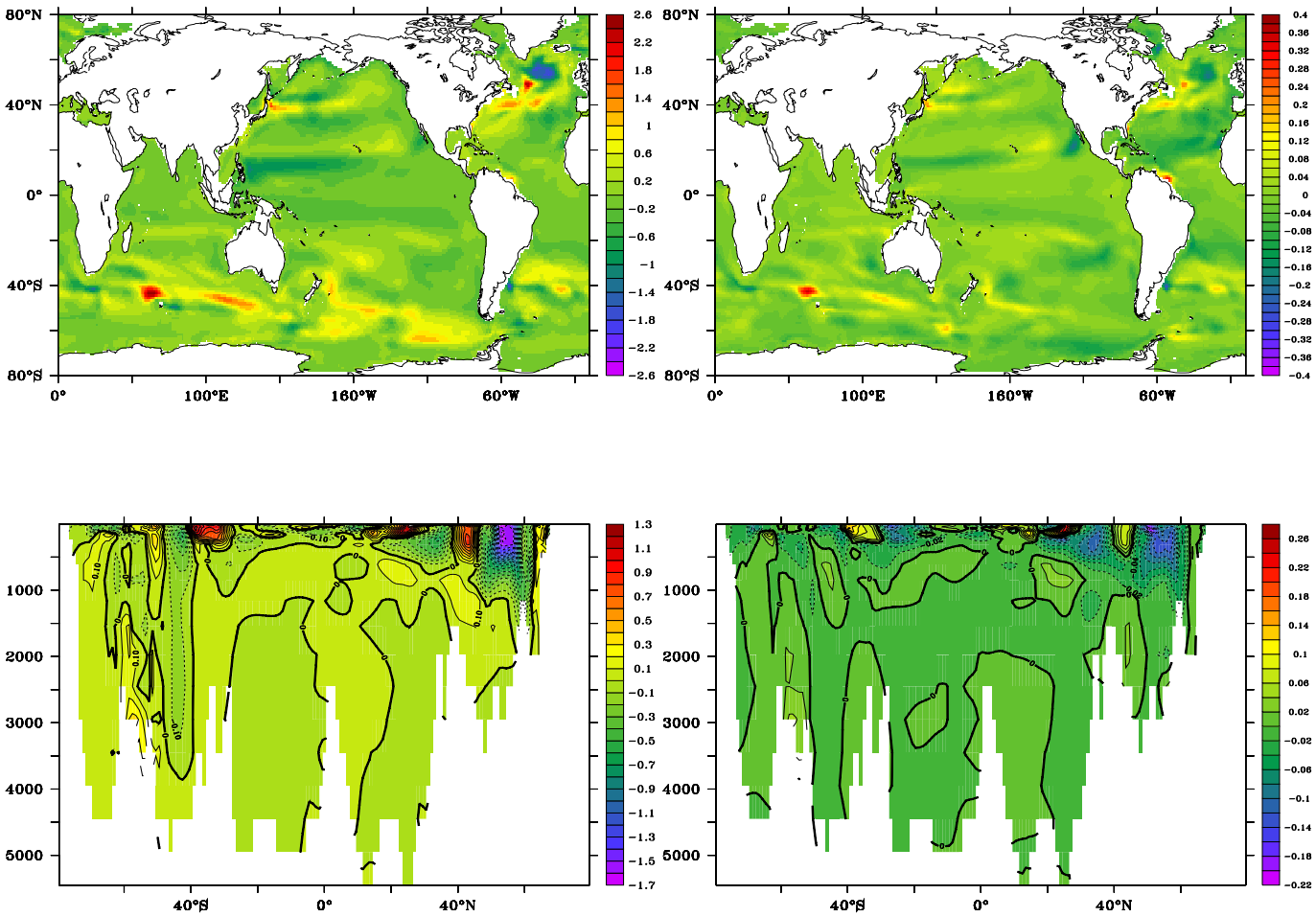
80°N
40°N
0°
40°S
80°S
0°
100°E
160°W
60°W
2.6
2.2
1.8
1.4
1
0.6
0.2
−0.2
−0.6
−1
−1.4
−1.8
−2.2
−2.6
0.4
0.36
0.32
0.28
0.24
0.2
0.16
0.12
0.08
0.04
0
−0.04
−0.08
−0.12
−0.16
−0.2
−0.24
−0.28
−0.32
−0.36
−0.4
1000
2000
3000
4000
5000
40°S
0°
40°N
1.3
1.1
0.9
0.7
0.5
0.3
0.1
−0.1
−0.3
−0.5
−0.7
−0.9
−1.1
−1.3
−1.5
−1.7
0.26
0.22
0.18
0.14
0.1
0.06
0.02
−0.02
−0.06
−0.1
−0.14
−0.18
−0.22

Figure 9:

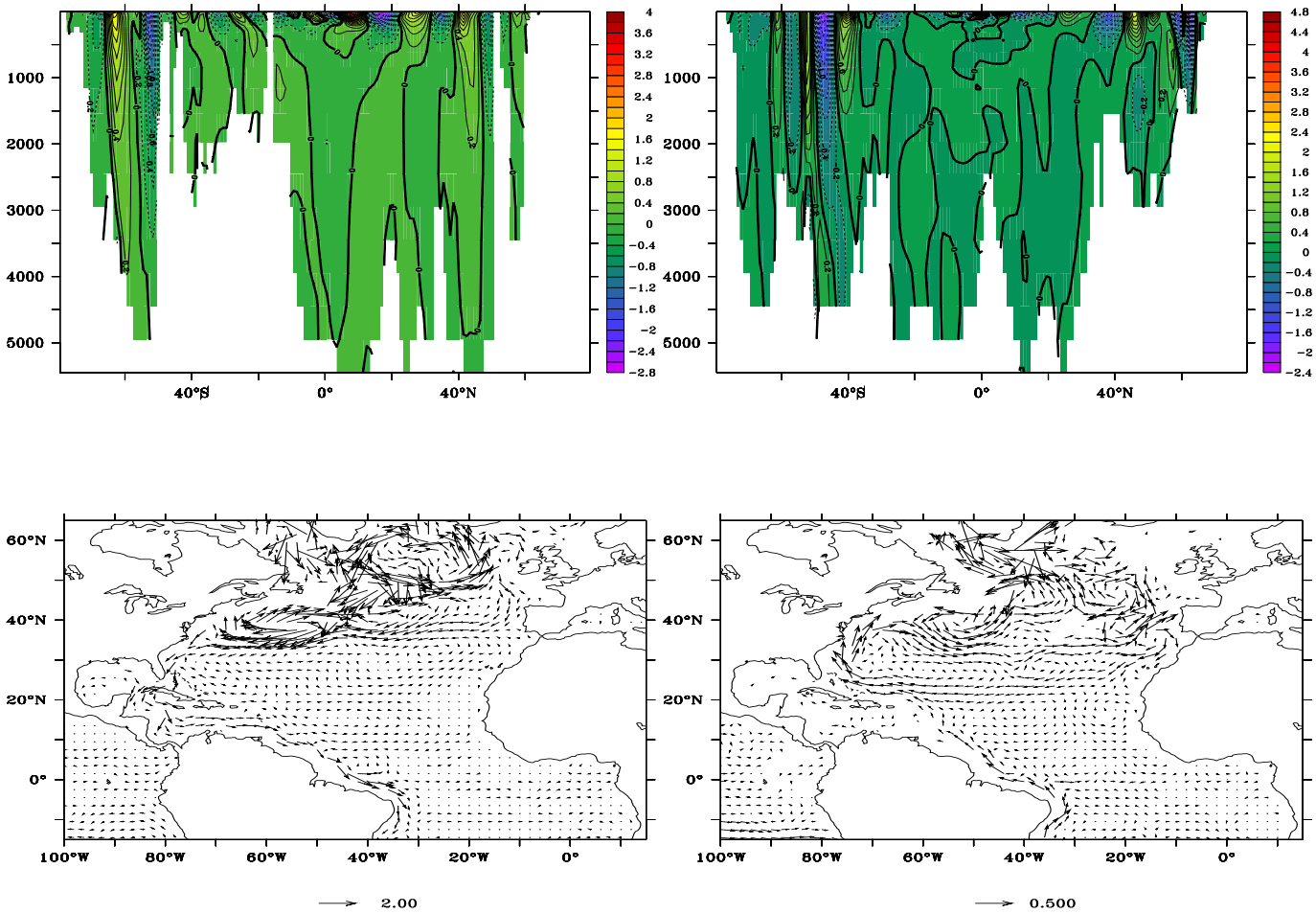
1000
2000
3000
4000
5000
40°S
0°
40°N
4
3.6
3.2
2.8
2.4
2
1.6
1.2
0.8
0.4
0
−0.4
−0.8
−1.2
−1.6
−2
−2.4
−2.8
4.8
4.4
4
3.6
3.2
2.8
2.4
2
1.6
1.2
0.8
0.4
0
−0.4
−0.8
−1.2
−1.6
−2
−2.4
60°N
40°N
20°N
0°
100°W
80°W
60°W
40°W
20°W
0°
2.00
0.500

Figure 10:

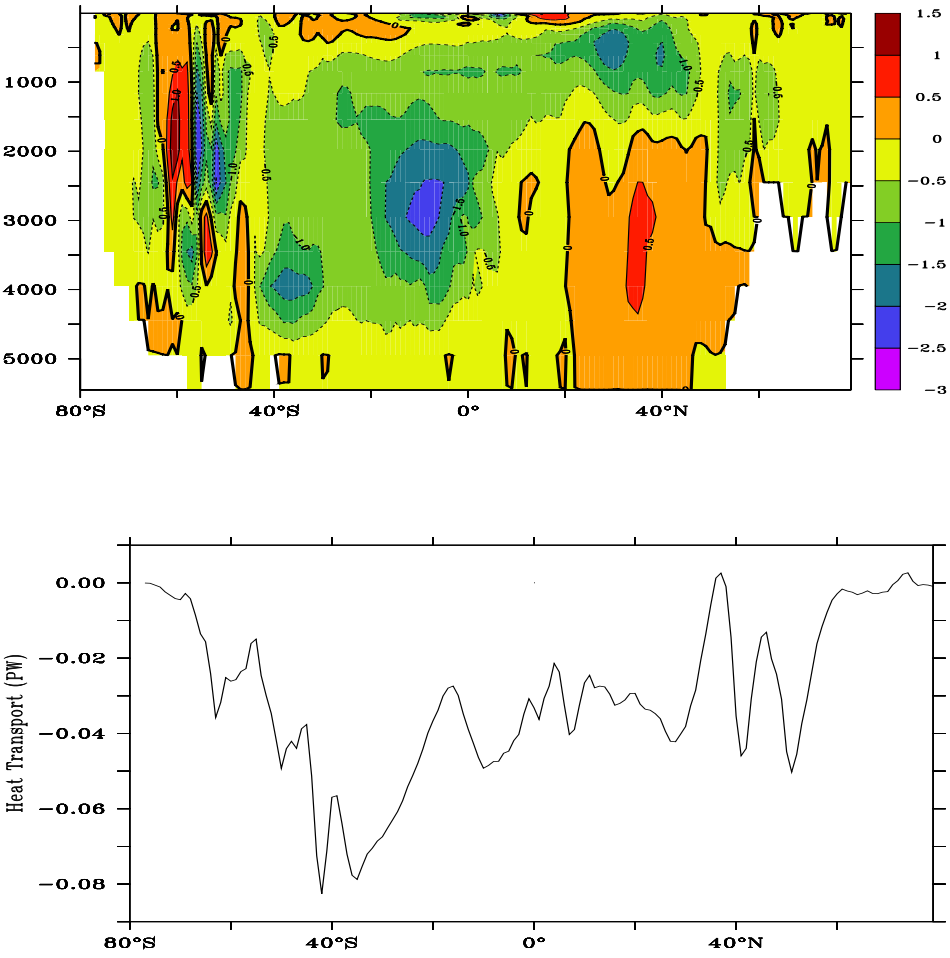
1000
2000
3000
4000
5000
80°S
40°S
0°
40°N
1.5
1
0.5
0
−0.5
−1
−1.5
−2
−2.5
−3
Heat Transport (PW)
0.00
−0.02
−0.04
−0.06
−0.08
80°S
40°S
0°
40°N

Figure 11: